

Numerical study on combustion dynamics of kerosene/GOx under supercritical condition

Jeongseok Kang * and Hong-Gye Sung**

*Department of Aerospace and Mechanical Engineering, Korea Aerospace University

*Goyang 412-791, South Korea

** Goyang 412-791, South Korea

Abstract

A large eddy simulation (LES) of supercritical combustion of kerosene/GOx is conducted using real gas thermodynamic relation and flamelet progress variable (FPV) method. The FPV method can capture dynamic flame structures (local extinction, re-ignition, flame stretching, and folding). In numerical simulation, the 'isolated flame' is observed with the flame extinction, re-ignition, and folding phenomenon. And the formation and extinction process of isolated flame is visualized and analysed with flame propagation images.

Nomenclature

C	Progress variable	Ψ	Progress variable flux
D	Diffusion coefficient	Q	Heat flux
E	Specific total energy	χ	Scalar dissipation rate
H	Energy flux	S	Strain rate
p	Pressure	δ	Kronecker delta
q	Heat flux	\dot{m}	Mass flux
t	Time	Subscript symbols	
u	Velocity	i, j	Spatial coordinate index
x	Spatial coordinate	F	Fuel
Y	Mass fraction	O	Oxidizer
Z	Mixture fraction	Superscript symbols	
σ	Viscous work	SGS	Subgrid scale
Φ	Scalar flux	$\overline{(\)}$	Time averaged
ρ	Density	$\widetilde{(\)}$	Favre averaged
τ	Shear stress	$(\)''$	Favre fluctuation
ω	Production rate		

1. Introduction

To improve both the performance and efficiency of liquid rocket engines, The higher operation pressure in rocket combustor is required with less instability. Propellants exceed their critical points and become supercritical state. In the supercritical state, thermodynamic properties, including heat capacity, thermodynamic relations, density, and thermal conductivity, clearly show different characteristics from traditional conditions of liquid or gas phase.

A liquid rocket engine has used liquid oxygen as an oxidizer and liquid hydrogen or hydrocarbon as a fuel. However, liquid hydrogen is too difficult to treat (e.g. store, transport, etc.) because of its extremely low temperatures. On the other hand, hydrocarbon fuel, like methane or kerosene, is a liquid phase at room temperature. They can be stored and charged with no subsidiary equipment. Besides, hydrocarbon fuel has economic advantages over liquid hydrogen. However, hydrocarbon type fuel is composed of hundreds of hydrocarbon compounds and thousands of reaction

mechanisms with a broad range of molecular weights, especially for kerosene-type fuel. For numerical analysis, handling the massive amounts of species and reactions is limited. Therefore, the use of a surrogate model is an attractive alternative.

In this study, a large eddy simulation(LES) is employed to predict the precise turbulent effect. As is well known, the LES directly calculate the large-scale motions, whereas eddies with smaller than the grid or filter size are modeled, like algebraic Smagorinsky or dynamic Smagorinsky model. In non-reacting case, the large scale flow is controlled via the geometry and the inlet conditions, whereas the small scale appear to be comparatively universal in terms of behaviour. On the other hand, in the reacting-case, chemical reactions occur at the molecular level. Therefore, in the reacting case, universal behaviour is not captured in the small-scale flow due to the chemical reaction. For this reason, in the reacting case, a turbulent combustion model should include the interaction between the turbulence effect and chemistry.

Many researchers have proposed the several turbulent combustion models to understand the turbulent combustion better using LES. The key in using such turbulent combustion model is to achieve closure for the filtered source term. Well known combustion model is eddy dissipation concept(EDC) model [1]. In recent years, several studies have shown that the stand EDC model over-predicts the maximum temperatures [2-3]. To overcome this drawback, modified EDC model was suggested using the functional expressions of the dependency of the EDC coefficients [4]. However, modified EDC model can not predict the re-ignition. And assumed probability density function model [5-6], transported probability density functions have been proposed [7-10]. However, very strong non-linearity caused inaccuracies in the interaction between turbulence and chemistry.

Instead, the present study employs the flamelet approach [11-12]. The flamelet approach assumes that the chemical time scale is much smaller than the turbulence time scale. In this manner, a turbulent flame can be considered as a combination of laminar flamelets. To apply the flamelet method, a flamelet library should be made up before numerical simulation. By solving the laminar flamelet equations, the laminar flame solution can be obtained. Then, this laminar flamelet solution is converted to turbulent flamelet solution using the Beta function PDF. Finally, the flamelet library is constructed as a function of mixture fraction, mixture fraction variance, and scalar variable (flame tracking variable). In the numerical simulation, mixture fraction conservation equation is solved instead handling the species equation. Mixture fraction variance and scalar variable are modeled using the similarity assumption in LES. By using the mixture fraction, mixture fraction variance, and scalar variable, the mass fraction of products is extracted from flamelet library. The flamelet method can save the computation costs and time with sustaining the accuracy.

In this study, the flame structure of kerosene/GOx is analyzed using flamelet equation and LES with flamelet progress variable(FPV) method under the supercritical condition. The FPV method overcomes the drawback of the steady laminar flamelet model using progress variable as flame strength parameter. To perform the FPV method, flamelet library should be constructed before numerical simulation. By solving the steady flamelet equation, laminar flamelet solution is obtained. Then, beta function PDF is applied to the laminar flamelet solution for turbulent effect. And real gas equation of state and transport properties are employed to the in-house code to capture the high-pressure effect.

2. Formulation

2.1 Governing equations

The filtered Favre-averaged mass, momentum, energy, mixture fraction and progress variable conservation equations are considered in numerical simulation as follows;

$$\frac{\partial \bar{\rho}}{\partial t} + \frac{\partial \bar{\rho} \tilde{u}_i}{\partial x_i} = 0 \quad (1)$$

$$\frac{\partial \bar{\rho} \tilde{u}_i}{\partial t} + \frac{\partial \bar{\rho} \tilde{u}_i \tilde{u}_j}{\partial x_j} = - \frac{\partial \bar{p}}{\partial x_i} + \frac{\partial (\tilde{\tau}_{ij} - \tau_{ij}^{SGS})}{\partial x_j}, \quad i = 1,2,3 \quad (2)$$

$$\frac{\partial \bar{\rho} \tilde{E}}{\partial t} + \frac{\partial (\bar{\rho} \tilde{E} + \bar{p}) \tilde{u}_i}{\partial x_i} = \frac{\partial}{\partial x_i} (\bar{q}_i + \tilde{u}_j \tilde{\tau}_{ij} - Q_i^{SGS} - H_i^{SGS} + \sigma_i^{SGS}) \quad (3)$$

$$\frac{\partial \bar{\rho} \tilde{Z}}{\partial t} + \frac{\partial (\bar{\rho} \tilde{u}_i \tilde{Z})}{\partial x_i} = \frac{\partial}{\partial x_i} \left(\bar{\rho} D \frac{\partial \tilde{Z}}{\partial x_i} - \Phi_i^{SGS} \right) \quad (4)$$

$$\frac{\partial \bar{\rho} \tilde{C}}{\partial t} + \frac{\partial (\bar{\rho} \tilde{u}_i \tilde{C})}{\partial x_i} = \frac{\partial}{\partial x_i} \left(\bar{\rho} D \frac{\partial \tilde{C}}{\partial x_i} - \Psi_i^{SGS} \right) + \dot{\omega}_C \quad (5)$$

The SGS terms are defined as

$$\tau_{ij}^{SGS} = \overline{\rho u_i u_j} - \bar{\rho} \tilde{u}_i \tilde{u}_j \quad (6)$$

$$Q_{ij}^{SGS} = (\bar{q}_i - \tilde{q}_i) \quad (7)$$

$$H_i^{SGS} = (\overline{\rho E u_i} - \bar{\rho} \tilde{E} \tilde{u}_i) + (\overline{\rho u_i} - \bar{\rho} \tilde{u}_i) \quad (8)$$

$$\sigma_i^{SGS} = \overline{u_i \tau_{ij}} - \bar{u}_i \bar{\tau}_{ij} \quad (9)$$

$$\Phi_i^{SGS} = \overline{\rho u_i \tilde{Z}} - \bar{\rho} \tilde{u}_i \tilde{Z} \quad (10)$$

$$\Psi_i^{SGS} = \overline{\rho u_i \tilde{C}} - \bar{\rho} \tilde{u}_i \tilde{C} \quad (11)$$

The mixture fraction conservation equation has many benefits than species conservation equation. In the case of kerosene-type fuel, hundreds of species exist in the combustion process. Solving hundreds of species equation for kerosene-type fuel is restrictive because of the computational cost and time. Instead, solving only mixture fraction equation can handle hundreds of species efficiently with flamelet library.

2.2 Thermodynamic and transport properties

To investigate the real gas effects, Soave-Redlich-Kwong(SRK) [13], Peng-Robinson(PR) [14], and Redlich-Kwong Peng-Robinson(RK-PR) [15] real gas equations are considered. Each equation of state is validated via a comparison with the extended corresponding states(ECS) at 80 bar. ECS is widely known as the most precise tool of thermodynamic properties prediction. Because the ECS has high computation cost, using the cubic EOS is an attractive alternative.

Figure 1, 2 shows the density and viscosity distribution for the JP-10 at 80 bar. In figure 1, the relative error of the difference from the ECS density is calculated as 15, 24 and 4% for the SRK, PR and RK-PR EOSes, respectively, at a kerosene inlet temperature of 443 K. In Figure 2, RK-PR EOS shows better accuracy than SRK and PR EOSes. Therefore, RK-PR EOS is implemented in this study.

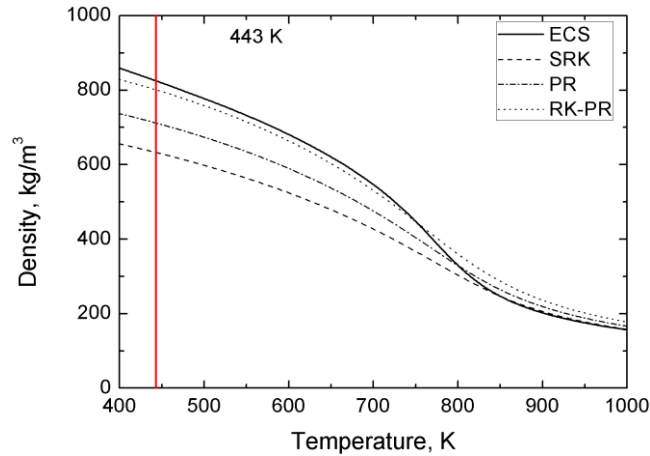


Figure 1 Density distribution for JP-10 at 80 bar

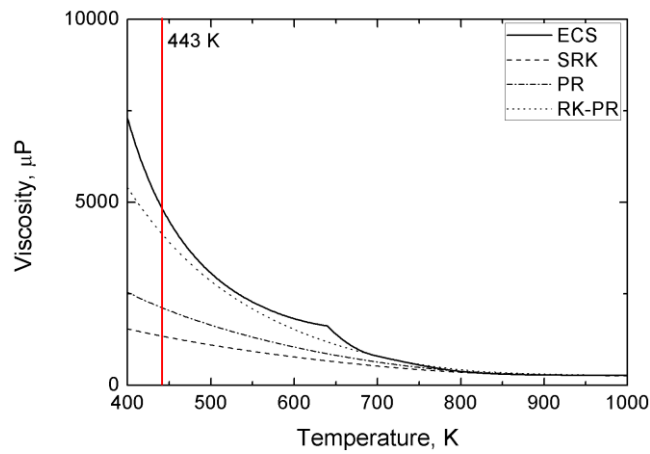


Figure 2 Viscosity distribution for JP-10 at 80 bar

Also, Chung's method [16] for viscosity and conductivity, and Takahashi's correlation [17] for diffusivity are employed to consider the high-pressure effect.

2.3 Flamelet library

In this study, to account for chemistry and turbulence interaction under the supercritical condition, the flamelet progress variable (FPV) method is considered. The FPV method can predict flame extinction, re-ignition, unsteady mixing effect and the lift-off phenomenon. The FPV method is comprised of three component steps. First, the laminar flamelet solution should be solved. Then, probability density function is used to the laminar flamelet solution to apply the turbulent effect. Lastly, numerical simulation is conducted with above flamelet library using the flamelet library parameters (mixture fraction, mixture fraction variance, flame tracking parameter).

In detail, firstly, steady laminar flamelet equation is solved at the operating condition with small chemical time scale assumption. Although the steady state is assumed, the steady flamelet solutions represent the various flame dynamics (e.g. the stretching and quenching of the flame). The steady flamelet equation is as follows;

$$\rho \frac{\chi}{2} \frac{\partial^2 Y_i}{\partial Z^2} + \dot{m}_i = 0 \quad (12)$$

By employing the scalar dissipation rate in the flamelet equation, an S-shaped curve which is the result of the strong non-linearity of the interaction of chemistry and mixing can be obtained. To solve the flamelet equation, a modified FLAMEMASTER code is implemented. RK-PR EOS is added to the original FLAMEMASTER code. As a kerosene type fuel, JP-10 kerosene surrogate model is employed [18]. A detailed chemistry mechanism for JP-10 has 53 species

and 263 reactions. After constructing the flamelet library, beta-function probability density function should be applied to add the turbulent effect. The beta-function PDF takes the following form.

$$P(Z; \tilde{Z}, \tilde{Z}''^2) = \frac{Z^{\alpha-1}(1-Z)^{\beta-1}}{\Gamma(\alpha)\Gamma(\beta)} \Gamma(\alpha + \beta) \quad (13)$$

Where Γ is the gamma function and α, β are defined as

$$\alpha = \tilde{Z} \left(\frac{\tilde{Z}(1-\tilde{Z})}{\tilde{Z}''^2} - 1 \right) \quad (14)$$

$$\beta = (1-\tilde{Z}) \left(\frac{\tilde{Z}(1-\tilde{Z})}{\tilde{Z}''^2} - 1 \right) \quad (15)$$

Then, the arbitrary properties are integrated with following equation.

$$\tilde{\phi}(\tilde{Z}, \tilde{Z}''^2, \tilde{C}) = \int_0^1 \int_0^1 \phi(Z, C) P(Z, C) dC dZ \quad (16)$$

where Z and C are independent. Also for simplicity's sake, the distribution of C is neglected with the assumption of a delta-function. Equation 16 is subsequently converted to equation (17).

$$\tilde{\phi}(\tilde{Z}, \tilde{Z}''^2, \tilde{C}) = \int_0^1 \int_0^1 \phi(Z, C) P(Z; \tilde{Z}, \tilde{Z}''^2) dZ \quad (17)$$

Next, the flamelet solution is integrated based on equation (17) and tabulated as a function of mixture fraction, mixture fraction variance, and progress variable. The selection of progress variable is very important in FPV method. It should represent the flame strength in numerical simulation. In this study, the progress variable is defined as the sum of CO_2 , CO , OH , H_2O mass fraction.

2.4 Numerical method

The governing equations outlined in the previous section are solved by implementing the finite volume method. The spatial discretization is calculated using a fourth order central differencing scheme. To suppress the numerical oscillation due to the central scheme, matrix dissipation model is employed [19]. Under the supercritical conditions, due to the high-density gradients, numerical instability can be shown for the interface. To overcome this problem, a unified treatment of the general fluid thermodynamics is established [20], which uses pressure decomposition and preconditioning techniques. For pseudo time advance, the 4 step Runge-Kutta scheme is employed. The code is paralleled using an MPI library for effective and fast calculations.

3. Results

3.1 Model description

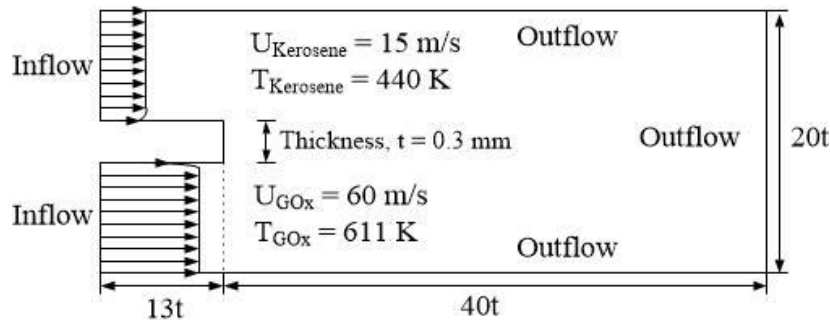


Figure 3 Geometry and boundary conditions

The computational domain and boundary conditions in this study is shown Figure 3. To understand the structure and the evolution of the supercritical kerosene/GOx combustion, the splitter shape above, which has five grids in the k -direction domain, is employed. The kerosene and gaseous oxygen flow into the combustor at 443K at 15m/s and 611K at 60m/s, respectively. The operating pressure is 80bar which is higher than the oxygen and kerosene's critical point, and the tip thickness is 0.3mm. The perturbation at inlet velocity is generated by a Gaussian random number with 5% intensity of the mean velocity.

3.2 S-shape at various pressures

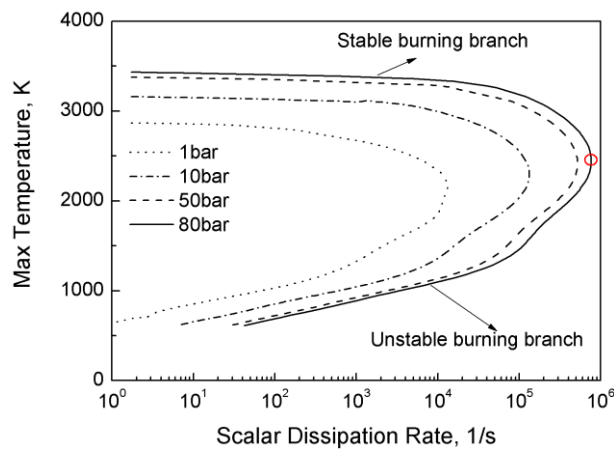


Figure 4 The S-shaped curve at various pressure to scalar dissipation rate

Figure 4 shows the maximum temperature distribution as a function of scalar dissipation rate at various pressures. The x-axis is a log scale, and the y-axis is a linear scale. The scalar dissipation rate controls mixing in non-premixed combustion because it controls the gradients of the mixture fraction, z . Also, different scalar dissipation levels lead to different flame structures. The scalar dissipation rate provides the connection between the mixing field and the combustion modeling. In Fig. 4, at the fixed pressure (10bar), the maximum temperature remains constant for a relatively small scalar dissipation rate (~ 1000), and the temperature decreases at a relatively larger rate until the extinction point is reached. Then, as the scalar dissipation rate decreases, the temperature continues to decrease. In addition, at the fixed scalar dissipation rate, as the pressure increases, the maximum temperature increases because of the dissociation. In higher pressure, the high pressure restrains the dissociation which decreases the flame temperature. To observe more detail, the middle strength flame is presented in Fig 5. The position of the middle flame is marked in Fig 4.

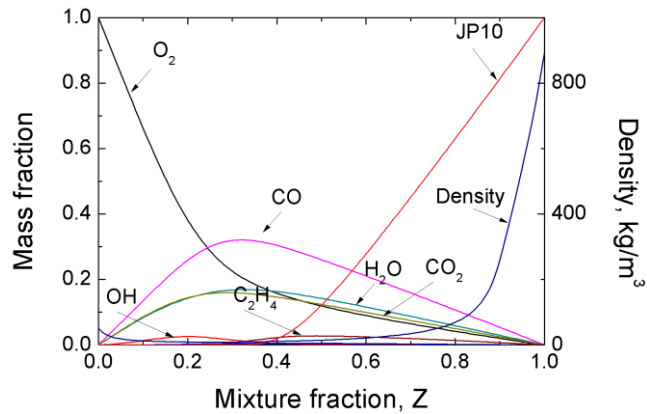


Figure 5 Major mass fraction and density distribution in mixture fraction space (intermediate flame)

Figure 5 shows the major mass fraction and density distribution in the mixture fraction space of middle strength flame. Oxygen is consumed partially, and fuel is consumed totally below mixture fraction 0.4. Product species also decreases than strongest flame. The results mean that as the progress variable decreases, the reaction occurs weakly, so species which is related to reaction diminish.

3.4 Flame structure

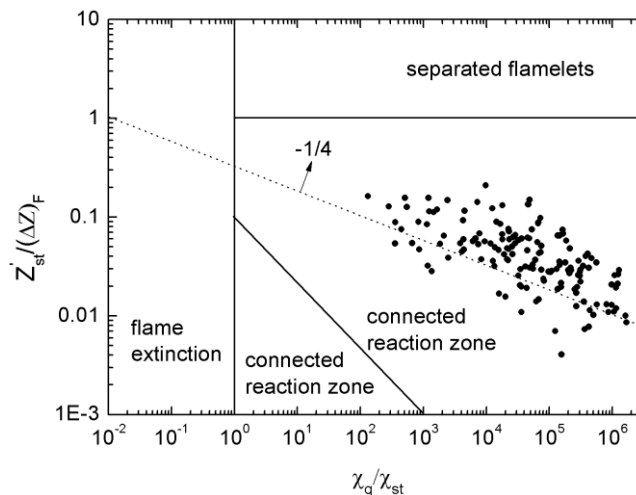


Figure 6 Diagram of non-premixed combustion in numerical results

In numerical simulation, the flame regime can be represented as shown in Fig. 6. The zone separation is proposed by Peters [21]. The x-axis shows quenching scalar dissipation rate to stoichiometric scalar dissipation rate. The y-axis represents the ratio between mixture fraction variance and stoichiometric mixture fraction. If y-axis is unity, mixture fraction variance is equal to the thickness of the reaction zone [21]. In higher than unity, separated flamelets are generated. To confirm the flame regime in numerical simulation, related properties are extracted at each cell points. In Fig. 6, all points are in connected reaction zone along the $-1/4$ slope. It means every flame shows strong flame motion. And there are no points in flame extinction zone. In Fig. 4, higher pressure makes the quenching scalar dissipation rate larger. In supercritical condition which is the operating condition in this study, quenching scalar dissipation rate is too high to reach in numerical simulation. Therefore, using the scalar dissipation rate as flame strength tracking parameter has drawback under the supercritical condition.

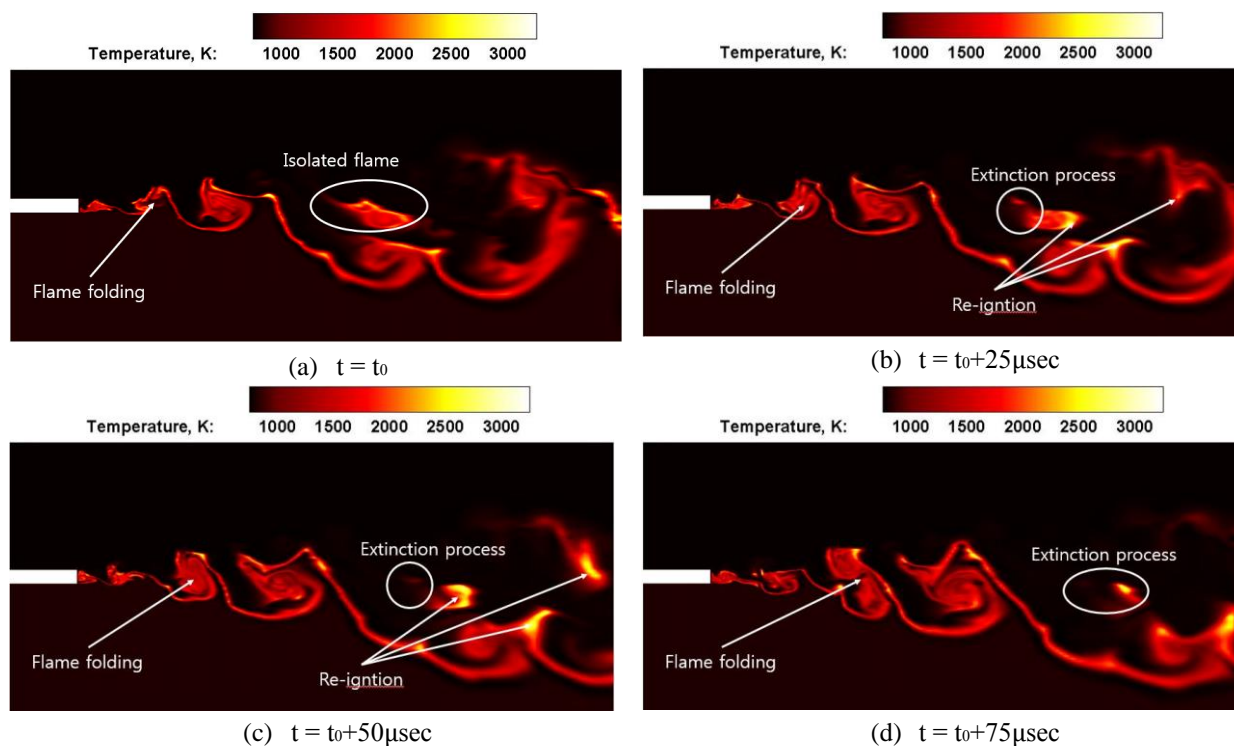


Figure 7 Temporal evolution of isolated flame with temperature contour

Behind the splitter tip, the fuel and oxygen streams with different velocities induce a Kelvin-Helmholtz type instability, which produces shedding oscillations at the interface between the fuel and oxygen streams. The strength of the vortex is higher than in the non-reacting case because of the rapid dilatation caused by the heat release. Figure 7 shows the temporal evolution of the isolated flame with temperature contours with 25 μsec interval. In Fig. 7 (a), the detached flame (isolated flame) and folding flames are observed. In Figs. 7 (b) through (d), the isolated flame shows the extinction and re-ignition processes in the isolated flame. As the isolated flame fully detached from main stream, the flame cannot maintain the combustion process because of the lack of the oxygen. On the other hand, since the right side of isolated flame is comprised of fuel and oxygen, the flame can be re-ignited, and it can survive combustion despite being separated from the mixing stream as long as it reaches the ignition temperature. The isolated flame is generated by the fuel vortex rotating in the counterclockwise direction. Accordingly, the left side can reach a combustible state relatively earlier than the right side. In addition, the right side can receive more oxygen just before separation, so it can be reignited later.

4. Conclusion

In this study, the flame structure of kerosene/ GO_x has been investigated using the LES and the FPV method under supercritical condition. The RK-PR EOS, Chung's method are considered to apply the high pressure effects for flamelet library and numerical simulation. The flame regime diagram shows that the steady flamelet method cannot predict the flame extinction or separated flame regime under supercritical condition. In numerical simulation, because of the high strength of vortex, isolated flame is generated behind the splitter tip. The isolated flame shows dynamic flame motion like local extinction, re-ignition, stretching. Even in same isolated flame, some part of the flame re-ignites and other part goes out because of the existence of the oxygen.

Acknowledgement

This work was supported by the Advanced Research Center Program (NRF-2013R1A5A1073861) through a National Research Foundation (NRF) of Korea grant funded by the Korean government (MSIP) contracted through the Advanced Space Propulsion Research Center at Seoul National University and by Ministry of Trade, Industry, and Energy and the Korea Aerospace Technology Research Association under project 10050539.

References

- [1] Chakraborty, D., Paul, P., Mukunda, M., 2000. Evaluation of combustion models for high speed H₂/air confined mixing layer using DNS data. *Combustion and Flame* 121:195-209.
- [2] Christo, F. C., Dally B. B., 2005. Modeling turbulent reacting jets issuing into a hot and diluted coflow, *Combustion and Flame* 142:117-129.
- [3] Frassoldati, A., Sharma, P., Cuoci, A., Faravelli, T., Ranzi, E., 2010. Kinetic and fluid dynamics modeling of methane/hydrogen jet flames in diluted coflow, *Applied Thermal Engineering* 30:376–383.
- [4] Parente, A., Malik, M. R., Contino, F., Cuoci, A., Dally, B. B., 2016. Extension of the Eddy Dissipation Concept for turbulence/chemistry interactions to MILD combustion, *Fuel* 163:98-111.
- [5] Baurle, R. A., Girimaji, S. S., 2003. Unsteady flow evolution and combustion dynamics of homogeneous solid propellant in a rocket motor, *Combustion and Flame* 131:131-148
- [6] Karl, S., Hannemann, K., Mack, A., Steelant, J., 2008. Ground testing of the hyshot II scramjet configuration in HEG, *AIAA Paper* 2008-2548
- [7] Baurle, R., Hsu, A., Hassan, H., 1995. Assumed Joint probability density function approach for supersonic turbulent combustion, *Journal of Propulsion and Power* 11:1132-1138
- [8] Mobus, H., Gerlinger, P., Bruggemann, D., 2003. Scalar and joint scalar-velocity-frequency monte carlo PDF simulation of supersonic combustion, *Combustion and Flame* 132:3-24
- [9] Koo, H., Donde, P., Raman, V., 2011. A quadrature-based LES/transported probability density function approach for modeling supersonic combustion, *Proceedings of the Combustion Institute* 33:2203-2210
- [10] Donde, P., Koo, H., Raman, V., 2012. A multivariate quadrature based moment method for LES based modeling of supersonic combustion, *Journal of Computational Physics* 231:5805-5821
- [11] Peters, N., 2000. *Turbulent Combustion*, Cambridge University Press.
- [12] Pitsch, H., 2006. Large-eddy simulation of turbulent combustion, *Annual Review of Fluid Mechanics* 38:453–482.
- [13] Soave, G., 1972. Equilibrium constants from a modified Redlich-Kwong equation of state, *Chemical Engineering science*, 27:1197-1203
- [14] Peng, D.Y., Robinson, D.B., 1976, A new two-constant equation of state, *Industry Engineering Chemical Fundamentals*, 15:59-64
- [15] Cismondi, M., Mollerup, J., 2005. Development and application of a three-parameter RK-PR equation of state, *Fluid Phase Equilibria*, 232:74-89
- [16] Chung, T., Ajlan, M., Lee, L., Starling, K., 1988. Generalized multiparameter correlation for nonpolar and polar fluid transport properties, *Industrial & Engineering Chemistry Research*, 27:671-679
- [17] Takahashi, S., 1974. Preparation of a generalized chart for the diffusion coefficients of gases at high pressures, *Journal of Chemical Engineering (Japan)* 7:417-420.
- [18] Li, S.C., Varatharajan, B., Williams, F.A., 2001. Chemistry of JP-10 ignition, *AIAA journal*, 12 :2351-2356
- [19] Swanson, R.C., Turkel, E., 1992. On central-difference and upwind schemes, *Journal of Computational Physics*, 101 :292-306
- [20] Zong, N., Yang, V., 2007. An efficient preconditioning scheme for real-fluid mixtures using primitive pressure-temperature variables, *International Journal of Computational Fluid Dynamics*, 21:217-230
- [21] Peters, N., 2004. *Turbulent Combustion*, Cambridge university press